OTC-28041-MS

Multirate Timestepping For Mooring Line Dynamics

Chee Meng Low, Lloyd's Register Global Technology Centre; Eddie Yin-Kwee Ng, Nanyang Technological University; Narasimalu Srikanth, Energy Research Institute @ NTU; Kie Hian Chua, Lloyd's Register Global Technology Centre

This paper was prepared for presentation at the Offshore Technology Conference Brasil held in Rio de Janeiro, Brazil, 24–26 October 2017.

Abstract

Direct time integration is a widely-used method for the analysis of loads and motions of mooring and floating systems. Nonlinear and transient effects can be easily accounted for in time domain analyses but it is a computationally expensive method, especially for explicit solvers which are limited by the timestep size to meet numerical stability requirements. There is potential in using multirate time to reduce computation times. This paper presents the development and evaluation of a multirate timestepping algorithm based on the Modified Euler integration method for the solution of mooring dynamics. The temporal synchronization as well as spatial boundary conditions needed for coupling the partitioned line segments with different spatial discretizations are presented. The stability parameters and gains in computational efficiency of the method are evaluated with numerical experiments based on a simple test case.

Introduction

Time domain simulation is an important tool for the analysis floating structure and mooring dynamic loads and motions. The strength of this approach is that the nonlinearities of the system responses can be readily accounted for, while its main drawback is its high computational cost. Central to the accuracy and efficiency of time-domain analysis approach is the choice of time marching algorithms which are broadly categorized into explicit and implicit types. Explicit methods are popular in existing codes but a major limitation is that their requirement for numerical stability typically imposes a smaller timestep, associated with the natural frequencies of the discrete line structure, than what might be needed for solution accuracy. Implicit methods, having superior stability characteristics enable larger timesteps to be taken, but the iterative solving of the nonlinear equation system require more computer memory and results in a higher computational cost per timestep compared to explicit methods. Thomas (1993) evaluated the numerical stability and accuracy of several timestepping algorithms, including both explicit and implicit methods, for use in a mooring dynamics code and found that while implicit algorithms allow larger timesteps to be used without the solution ‘blowing up", the solution accuracy deteriorates quickly with larger timesteps, hence diminishing the supposed advantage that implicit algorithms have over explicit ones.

The discretization used in a simulation of cable structures such as risers and moorings is an important factor for solution accuracy and mesh refinement may be needed in areas of large gradients (Det Norske Veritas, 2003; Elsacker, 1989), when large tension fluctuations (Bai, 2001) are experienced, and when moorings of low bending stiffness (Gobat, 2000) are used. The results in a structural model having varying nodal densities within a single line. The difference between the fine and coarse mesh sizes enlarges the separation between the largest and smallest eigenvalues of the effective stiffness matrix and gives rise to a stiff problem. For multisegmented mooring lines, the different material characteristics and discretizations for each segment result in different natural frequencies. In both cases, a monolithic, explicit timestepping strategies will use a single timestep for the entire structure that is limited by the highest natural frequency in the structural model. In contrast, a multirate timestepping method enables different timesteps to be used in different segments of the structural model. Reduction in the computational cost is achieved by using smaller timesteps only where they are required for stability or accuracy.

In a pioneering work on multirate schemes, Andrus (1979) describes a dualrate integration procedure for two coupled subsystems marched forward in time with different timesteps, using the classical fourth- order Runge Kutta (RK4) method for each subsystem, and Taylor series extrapolation to obtain the values for the interacting variables during intermediate stage evaluations. Multirate integration methods are widely studied and used in electric circuit simulations (A Bartel, Gunther, and Rentrop, 2002; Andreas Bartel, 2001; Günther, Kværnø, and Rentrop, 2001; Kavaerno and Rentrop, 1999; Verhoeven, Guennouni, ter Maten, and Mattheij, 2005), due to the inherent separation in the timescales and the intermittent latency of connected digital and analogue components. Gander and Halpern (2013) zequations. In addition to electric circuits, multirate algorithms have been applied to simulation of multibody systems (J. Chang, Ploen, Sohl, and Martin, 2004; Shome, Haug, and Jay, 2004; Tomulik and Frâczek, 2011). The crucial issues of multirate timestepping include numerical stability and the coupling and synchronization strategy between subsytems.

In this paper, a multirate timestepping algorithm is applied to the dynamic simulation of mooring lines. The base time-integration method is the modified-Euler (ME) method. A homogenous line structure with spatially varying discretization will be used as a test case to evaluate the stability parameters and computational gains of the mulitrate method.

Mooring Line Model

Equation of Motion

The mooring structure is discretized as shown in Figure 1 and the mooring structural dynamics equation of motion for a discrete nodal element *i* is,

$$\boldsymbol{M}_{total,i}\ddot{\boldsymbol{r}}_i = \left(\boldsymbol{M}_i + \boldsymbol{M}_{a,i}\right)\ddot{\boldsymbol{r}}_i = \sum \boldsymbol{F} = \boldsymbol{W}_i + \boldsymbol{T}_i + \boldsymbol{F}_{D,i} + \boldsymbol{F}_{I,i} + \boldsymbol{F}_{B,i} + \boldsymbol{F}_{S,i} \tag{1}$$

where $\boldsymbol{M}_i$, $\boldsymbol{M}_{a,i}$, and $\boldsymbol{W}_i$ are respectively the structural and added mass matrices and weight vector, $\ddot{\boldsymbol{r}}_i$ is the acceleration vector, $\boldsymbol{T}_i$ accounts for axial tension forces, $\boldsymbol{F}_{D,i}$ and $\boldsymbol{F}_{I,i}$ represent fluid viscous drag and inertial forces, $\boldsymbol{F}_{B,i}$ is the seabed force vector and $\boldsymbol{F}_{S,i}$ accounts for structural damping.

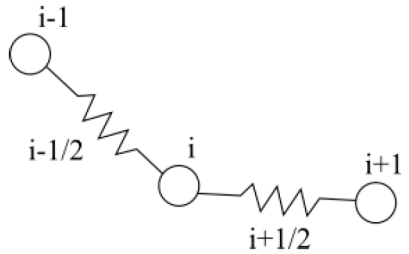

Figure 1—Discretization of Line Structure

Structural Mass and Weight

A lumped parameter approach is used to spatially discretize the mooring structure. Following the schematic shown in Figure 1, the mass of each node is,

$$m_i = \frac{1}{2} \sum_{\eta=\frac{1}{2},-\frac{1}{2}} m_{i+\eta} \tag{2}$$

where i is the nodal index and $i + \eta$, for $\eta = \left\{\frac{1}{2}, -\frac{1}{2}\right\}$, are the elemental indices on either side of the node, and m is mass. $\boldsymbol{M_i}$ is the diagonal structural mass matrix,

$$\boldsymbol{M_i} = \boldsymbol{I} m_i \tag{3}$$

and $\boldsymbol{I}$ is the usual 3×3 identity matrix. Considering the effects of buoyancy, the weight of each node in seawater is,

$$\boldsymbol{W}_i = \left(m_i - \frac{1}{2} \rho_w \sum_{\eta=\frac{1}{2},-\frac{1}{2}} A_{i+\eta}\, l_{i+\eta} \right) g\, \hat{\boldsymbol{k}} \tag{4}$$

where $\boldsymbol{W_i}$ is the nodal weight vector, $\hat{\boldsymbol{k}}$ is the unit vector in the vertical direction, ρ_w is the density of seawater, g is the gravitational acceleration constant and A and l are the elemental cross sectional area and unstretched length respectively.

Tension

The nodal tension force is given by,

$$\boldsymbol{T}_i = \sum_{\eta=\frac{1}{2},-\frac{1}{2}} \mathrm{sgn}(\eta)\, T_{i+\eta}\, \hat{\boldsymbol{e}}_{i+\eta} \tag{5}$$

where $\hat{\boldsymbol{e}}$ is the elemental unit vector of the $i + \eta$ element and T is the elemental tension force that is calculated using a bilinear model proposed by Huang and Vassalos (1993) which accounts for the inability of the lines to take compression loads,

$$T_{\mathrm{i}+\eta} = \begin{cases} \dfrac{EA_{i+\eta}}{l_{i+\eta}} \left(l'_{i+\eta} - l_{i+\eta} \right), & l > l' \\ 0, & l \le l' \end{cases} \tag{6}$$

where T is the tension, E is the material elastic modulus, and l' is the stretched elemental length calculated from the instantaneous nodal positions.

Hydrodynamic Forces

The hydrodynamic forces acting on a line are calculated using Morison's equation, and for a segment of length L and nominal cross-sectional area A and diameter D is,

$$F_M = \underbrace{-\rho_w A L C_a}_{\boldsymbol{M_a}} \ddot{r} + \underbrace{\rho_w A L (C_a + 1) u}_{\boldsymbol{F_I}} + \underbrace{\frac{1}{2} \rho_w D L C_d |u - \dot{r}| (u - \dot{r})}_{\boldsymbol{F_D}} \tag{7}$$

where C_a and C_d are the added mass and viscous drag force coefficients, $\dot{u}$ is the fluid acceleration, and u and $\dot{r}$ are the fluid and structural velocities at the line segment, and account for the $\boldsymbol{M_a}$, $\boldsymbol{F_I}$ and $\boldsymbol{F_D}$ terms in

Equation 1. For compactness Equation 8 is shown in scalar form, but are implemented as vector quantities and the contributions to each term are from line normal and tangential components.

Seabed Force

The seabed interaction force consists of the vertical seabed reaction,R_B, and friction forces, $\boldsymbol{F}_{B,fric}$,

$$\boldsymbol{F}_B = R_B\,\hat{\boldsymbol{k}} + \boldsymbol{F}_{B,fric} \tag{8}$$

The vertical reaction force follows the spring mattress model as proposed by Webster (1995),

$$R_B = \begin{cases} m_i g, & z_i < z_B \\ -\mathrm{k}_{B,i}(z_i - z_B) + \mathrm{m}_i g, & z_B \le z_i \le z_B + \dfrac{d_i}{2} \\ 0, & z_i > \dfrac{d_i}{2} \end{cases} \tag{9}$$

where z_B is the seabed elevation, z_i is the nodal vertical distance from the seabed, d_i is the outer diameter of the line segment, and seabed spring stiffness, $k_{B,i}$ is $2m_ig/d_i$. The seabed friction is assumed to be isotropic and is calculated via a Coulomb-friction model (see e.g. Elosta, Huang, and Incecik, 2016; Liu and Bergdahl, 1997; Yu and Tan, 2006) for the nodes which experience non-zero vertical reaction.

$$\boldsymbol{F}_{B,fric} = \begin{cases} -c_B\dot{\boldsymbol{r}} & , c_B|\dot{\boldsymbol{r}}| \le \mu_s R_B,\ \ R_B > 0 \\ -\mu_s R_B \dfrac{\dot{\boldsymbol{r}}}{|\dot{\boldsymbol{r}}|} & , c_B|\dot{\boldsymbol{r}}| > \mu_s R_B,\ \ R_B > 0 \\ 0 & , R_B = 0 \end{cases} \tag{10}$$

where μ_s is static friction coefficient, and c_B is the seabed critical damping coefficient

$$c_B = 2\sqrt{k_{B,i}m_i} \tag{11}$$

Hence, the magnitude of the friction force is limited by the static friction limit and acts in the direction opposite to the nodal velocity.

Structural Material Damping

The material damping in a line element is formulated as,

$$\boldsymbol{F}_{S,i} = \sum_{\eta=\frac{1}{2},-\frac{1}{2}} \mathrm{sgn}(\eta)\; C_{S,i+\eta}\left|\Delta\dot{\boldsymbol{r}}_{i+\eta}\right| \hat{\boldsymbol{e}}_{i+\eta} \tag{12}$$

where $C_{s\eta}$ is the material damping coefficient and $\Delta\dot{\boldsymbol{r}}_{i+\eta}$ is the relative velocities between the nodes bounding the element.

Multirate Timestepping Integration

Overview of Multirate Methods

After performing spatial discretization of the mooring line structure, a system of ordinary differential equations is obtained, as shown in Equation 13, where y is the state vector and y_0 is the initial condition. The dynamics of the mooring structure is then obtained by solving the initial value problem with suitable time integration schemes.

$$\dot{y} = f(t, y), \qquad y(t_0) = y_0, \qquad y \in \mathbb{R}^n \tag{13}$$

The system can be separated into k partitions,

$$\begin{aligned} \dot{y}_1 &= f_1(y_1, y_2, \dots, y_k) \\ \dot{y}_2 &= f_2(y_1, y_2, \dots, y_k) \\ &\vdots \\ \dot{y}_k &= f_k(y_1, y_2, \dots, y_k) \end{aligned} \tag{14}$$

where y - $[y_i, y_2, \dots, y_k]^T$, $y_i \in \mathbb{R}^{n_i}$, and $n = \sum_{i=0}^{k} n_i$, where n_i is the degrees of freedom in Partition i and n is the total number of degrees of freedom of the system. Each partition can have its own timestep and time integration algorithm, different from the other partitions, and information exchange between itself and the partitions coupled to it takes place at synchronization points in time. This requires that the timestep of each partition be multiples of those coupled to it. This is illustrated in Figure 2 for two coupled partitions, where the macro timestep H is p times that of the micro timestep, h.

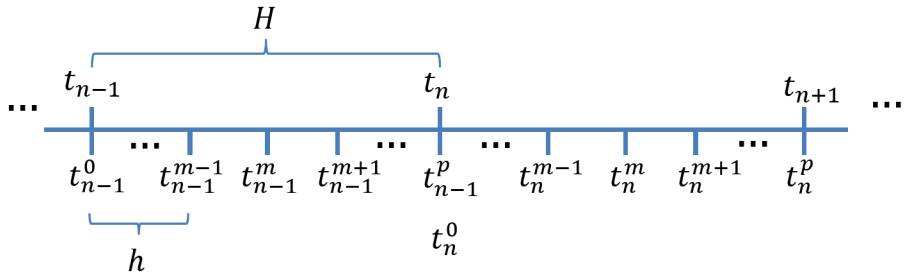

Figure 2—Macro and micro timesteps. Adapted from Leyendecker and Ober-Blobaum (2013)

In the context of mooring and cable structures, the allowable timesteps are determined by the structural stiffness and spatial discretization which may vary along the line structure. A fine discretization or high structural stiffness will result in a smaller timestep, which can be calculated from the eigenvalues of the effective stiffness matrix (Bathe, 1996). An example of this is shown in Figure 3, which consists of two regions of different nodal densities, Partitions C and F, the stable timesteps for each region will differ from each other. A monolithic integrator will be restricted to using the smaller stable timestep for the entire structure even though the timestep for the region with the coarser discretization may be larger without incurring a large penalty in terms of accuracy.

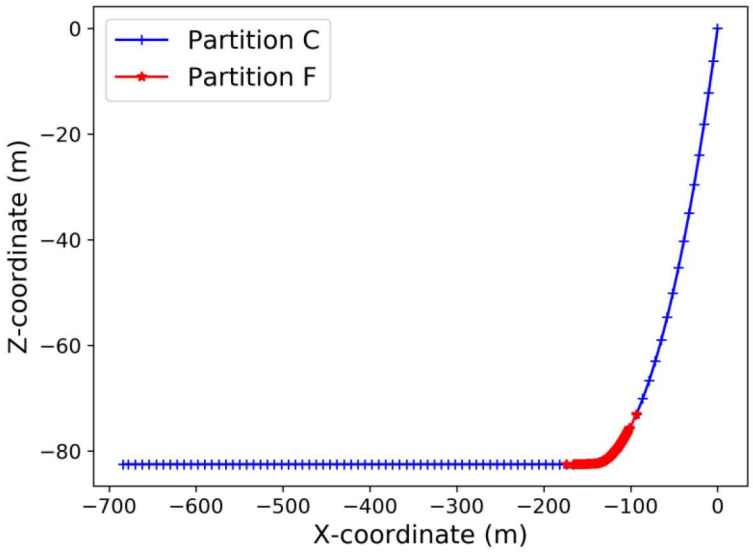

Figure 3—Test Case Mooring Line Initial Line Shape

The time-integration of the coupled components may take place sequentially or in parallel. For the sequential approach, a choice may be made to advance the slow or fast changing components first. During the integration of this first batch of partitions, information on the states of the coupled components may be required and these are either obtained from extrapolation or taken from the last known values. The other partitions are then sequentially advanced in time using the information available from the components that have already been advanced in time and interpolating as necessary. In a segregated approach, the integration of all the components may take place simultaneously, using extrapolation methods such as linear, polynomial or rational function extrapolation (Arnold, 2007; Gear and Wells, 1984) to obtain the values for the coupled state variables. The synchronization of the components then take place at the end of a macrostep, H.

Proposed Multirate Scheme

The slowest and fastest-first approaches are methods in which the partitions are sequentially advanced in time and the order of integration is determined based on the relative timescales of the partitions. Gear and Wells (1984) briefly explain the merits and drawbacks of the two approaches. The slowest-first approach will be used in the present study. The base integration algorithm is the modified-Euler (Hahn, 1991) procedure,

$$\boldsymbol{y}^{n+1} = \begin{bmatrix} \boldsymbol{r} \\ \dot{\boldsymbol{r}} \end{bmatrix}^{n+1} = \begin{bmatrix} \boldsymbol{r} \\ \dot{\boldsymbol{r}} \end{bmatrix}^{n} + \left(\begin{bmatrix} 0 & 0 \\ 0 & 1 \end{bmatrix} \begin{bmatrix} \dot{\boldsymbol{r}} \\ \ddot{\boldsymbol{r}} \end{bmatrix}^{n} + \begin{bmatrix} 1 & 0 \\ 0 & 0 \end{bmatrix} \begin{bmatrix} \dot{\boldsymbol{r}} \\ \ddot{\boldsymbol{r}} \end{bmatrix}^{n+1} \right) \Delta t \tag{15}$$

where $\boldsymbol{r}$ and $\dot{\boldsymbol{r}}$ are the nodal position and velocity vectors. The acceleration vector, $\ddot{\boldsymbol{r}}$, is calculated as,

$$\ddot{\boldsymbol{r}}^{n} = \boldsymbol{M}_{\boldsymbol{total}}{}^{-1} \sum \boldsymbol{F}\left(\boldsymbol{y}^{n}\right) \tag{16}$$

The ME algorithm can be conveniently paired with the slowest-first approach. To illustrate this, consider a two-partition system, for which Equation 18 can be written as

$$\begin{aligned} \dot{\boldsymbol{y}}_L &= \boldsymbol{f}_L(t, \boldsymbol{y}_A, \boldsymbol{y}_L) \\ \dot{\boldsymbol{y}}_A &= \boldsymbol{f}_A(t, \boldsymbol{y}_L, \boldsymbol{y}_A) \end{aligned} \tag{17}$$

where $\boldsymbol{y}_L$ and $\boldsymbol{y}_A$ represent the slow components and fast components respectively. Using the ME method, the multirate method proceeds in the following steps:

1. Advance the slow components to $t_{n+1} = t_n + H$,

$$\boldsymbol{y}_L^{n+1} = \begin{bmatrix} \boldsymbol{r}_L \\ \dot{\boldsymbol{r}}_L \end{bmatrix}^{n+1} = \begin{bmatrix} \boldsymbol{r}_L \\ \dot{\boldsymbol{r}}_L \end{bmatrix}^{n} + \left(\begin{bmatrix} 0 & 0 \\ 0 & 1 \end{bmatrix} \begin{bmatrix} \dot{\boldsymbol{r}}_L \\ \ddot{\boldsymbol{r}}_L \end{bmatrix}^{n} + \begin{bmatrix} 1 & 0 \\ 0 & 0 \end{bmatrix} \begin{bmatrix} \dot{\boldsymbol{r}}_L \\ \ddot{\boldsymbol{r}}_L \end{bmatrix}^{n+1} \right) H \tag{18}$$

where

$$\ddot{\boldsymbol{r}}_L^n = \boldsymbol{M}_L{}^{-1} \boldsymbol{f}_L(\boldsymbol{y}_L^n, \boldsymbol{y}_A^n) \tag{19}$$

2. Advance the fast components to $t_n^{m+1} = t_n^m + h$, $m = \{0,1,\dots,p-1\}$,

$$\boldsymbol{y}_A^{m+1} = \begin{bmatrix} \boldsymbol{r}_A \\ \dot{\boldsymbol{r}}_A \end{bmatrix}^{m+1} = \begin{bmatrix} \boldsymbol{r}_A \\ \dot{\boldsymbol{r}}_A \end{bmatrix}^{m} + \left(\begin{bmatrix} 0 & 0 \\ 0 & 1 \end{bmatrix} \begin{bmatrix} \dot{\boldsymbol{r}}_A \\ \ddot{\boldsymbol{r}}_A \end{bmatrix}^{m} + \begin{bmatrix} 1 & 0 \\ 0 & 0 \end{bmatrix} \begin{bmatrix} \dot{\boldsymbol{r}}_A \\ \ddot{\boldsymbol{r}}_A \end{bmatrix}^{m+1} \right) h \tag{20}$$

where

$$\ddot{\boldsymbol{r}}_A^m = \boldsymbol{M}_{\boldsymbol{A}}{}^{-1} \boldsymbol{f}_A(\widetilde{\boldsymbol{Y}}_L^m, \boldsymbol{y}_A^m) \tag{21}$$

and $\widetilde{\boldsymbol{Y}}_L^m$ represents the interpolated values of $\boldsymbol{y}_L$ at the mth microstep that are linearly interpolated as

$$\widetilde{\boldsymbol{Y}}_L^m = \boldsymbol{y}_L^n + mh \left(\frac{\boldsymbol{y}_L^{n+1} - \boldsymbol{y}_L^n}{H} \right) \tag{22}$$

Therefore, to obtain $\boldsymbol{y}_L^{n+1}$ only $\boldsymbol{y}^n = [\boldsymbol{y}_A^n, \boldsymbol{y}_L^n]^{\boldsymbol{T}}$ at the previous synchronization point is needed because there are no intermediate stages between $\boldsymbol{t_n}$ and $\boldsymbol{t_n}_{+1} = \boldsymbol{t_n} + \boldsymbol{H}$ which require the values of $\boldsymbol{y}_A$ for function evaluations. The intermediate stage function evaluations in higher order Runge-Kutta schemes require $\boldsymbol{y}_A$ values to be supplied, which are obtained from linear extrapolation (Arnold, 2007), higher order polynomial or rational extrapolation (Hull, Enright, and Fellen, 1972), or Taylor series expansions. However, there are complexities involved in the choice of extrapolation method which may jeopardize solution stability (Gear and Wells, 1984; Gunther and Rentrop, 1993). Therefore, the ME scheme is good choice for the base integration method in a staggered multirate scheme. After the slow partition is advanced in time using a stable macro-timstep, its values at the microsteps can be obtained by interpolation at any temporal resolution.

Spatial Coupling

A schematic of the nodal mapping between the singlerate mooring line and the multirate segments as well as the spatial coupling between coupled multirate partitions is shown in Figure 4, where $\boldsymbol{y}$ is the state vector of the entire line containing all the nodes, $\boldsymbol{y}_1$ is the state vector of one partition with a timestep of $\boldsymbol{h}_1$, and $\boldsymbol{y}_2$ is the state vector of a partition coupled to $\boldsymbol{y}_1$ with a timestep of $\boldsymbol{h}_2$.

There is an overlap at the interface between the two partitions, where the ends of each partition obtain the boundary conditions for its own time advancement from the coupled neighbor partition. For Partition 1 with state vector $\boldsymbol{y}_1$, these are obtained from $\boldsymbol{y}_{2,1}$ and $\boldsymbol{y}_{2,-2}$, using the interpolation method described in the previous section. Similarly, to advance $\boldsymbol{y}_2$, the boundary values for $\boldsymbol{y}_{2,0}$ and $\boldsymbol{y}_{2,-1}$ are obtained from $\boldsymbol{y}_{1,j-1}$ and $\boldsymbol{y}_{1,j+2}$ respectively. At the end of each macrostep, the state values of the boundary nodes for both partitions are then updated from coupled partition. Hence the synchronization takes place at each macrostep and the dynamics of the boundary nodes are therefore calculated in the neighbour partition.

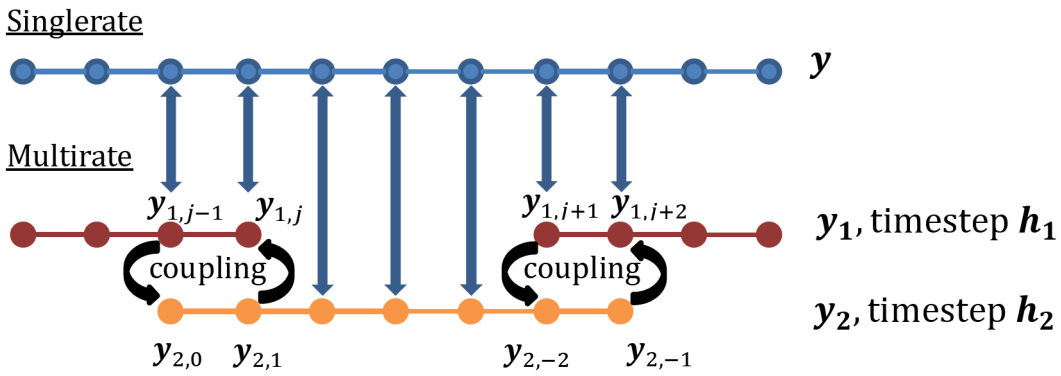

Figure 4—Spatial Coupling Between Partitions

Test Case Setup

Thomas (1993) found that impact loads associated with seabed contact gave rise to spurious tension fluctuations at the fairlead, and that a reduction in the nodal mass aided in reducing the impact loads. Central to dealing with this problem are various seabed contact models which prescribe a seabed support force profile that gradually increases as nodes approach the seabed (Ghadimi, 1988; Low and Langley, 2008) as well as providing vertical damping force (Boom, 1985; Z. Chang et al., 2012; Kurian, Yassir, Ng, and Harahap, 2013). These models rely on the use of constants that need to be tuned for a particular simulation to mitigate the effect of the impact force due to nodal grounding. However, as Thomas suggested, by reducing the mass of nodes that impact the seabed, the spurious tension fluctuations may be reduced. To investigate the effectiveness of this approach, we will use refined nodal elements at the touchdown point. The presence of two regions with different nodal densities and thus stable timesteps also allows us to the apply the multirate algorithms and evaluate their performance.

Test case 1.3.1 as specified in the blind test study conducted by Brown and Mavrakos (1999), one of the test cases used in the validation phase of this work, which prescribes an imposed sinusoidal fairlead motion of 5.4 meters and a period of 10 seconds, will be used. The water depth is 82.5 meters and the length of the mooring line is 711.3 meters. The material properties including mass and hydrodynamic coefficients of the mooring line is homogeneous for its entire length. With the spring mattress seabed model by Webster (1995), fine discretization at the touchdown point is needed to avoid tension fluctuations arising from nodal grounding. Appendix A shows the discretizations of the mooring line. There are two regions of different refinement levels, which are also separate partitions in a multirate timestepping scheme. In the vicinity touchdown point is the segment with increased nodal density and a correspondingly smaller element length, hereafter referred to as Partition F, that is coupled to Partition C which has a comparatively lower nodal density and larger element length.

The nomenclature that will be used to describe the simulation parameters as well as evaluation of the performance are listed in Table 1. The effect of varying the nodal density and size of Partition F on the stability, accuracy and computational efficiency of the multirate scheme, in comparison to their corresponding singlerate variants was investigated. For these purposes, several discretizations of the mooring line, as shown in Table 2 were used. E1 to E6 are a series of tests in which the length of Partition F was varied between 40.3m and 65.3m. In the R1 to R4 series of tests, the length of Partition F was kept constant at 55.3m with a progressive increase in nodal density as its element length was reduced from 1.257m to 0.498m. Appendix A shows the line discretizations for the series of tests conducted.

Table 1—Nomenclature of Multirate Simulation and Performance Evaluation Parameters

Symbol	Definition	Symbol	Definition
Δt_c	Partition C timestep, macro-timestep	Δt_f	Partition F timestep, micro-timestep
$\Delta t_{c,max}$	Partition C maximum stable timestep	$\Delta t_{f,max}$	Partition F maximum stable timestep
a_c	Partition C timestep ratio, $\Delta t_c/\Delta t_{c,max}$	a_f	Partition timestep ratio, $\Delta t_f/\Delta t_{f,max}$
β	Computational time speedup factor, $\frac{\text{Wall clock time}_{multirate}}{\text{Wall clock time}_{singlerate}}$	κ	Stiffness factor, ratio between Partition C and F maximum stable timesteps, $\frac{\Delta t_{c,max}}{\Delta t_{F,max}}$
P	Number of microsteps within a macrostep, $\Delta t_c = p\Delta t_f$		

Table 2—Discretization Parameters for E1 to E6 (expansion of Partition F size) and R1 to R4 (progressive refinement of Partition nodal density) tests

Discre-tization	Partition F			Partition C		
	Total length (m)	Element length (m)	No. of Nodes	Total length (m)	Element length (m)	No. of Nodes
El	40.3	0.498	89	671	8	86
E2	45.3	0.498	100	666	8	85
E3	50.3	0.498	111	661	8	85
E4	55.3	0.498	122	656	8	85
E5	60.3	0.498	133	651	8	84
E6	65.3	0.498	144	646	8	83
R1	55.3	1.257	48	656	8	85
R2	55.3	1.005	61	656	8	85
R3	55.3	0.747	81	656	8	85
R4	55.3	0.498	122	656	8	85

To evaluate the stability of the multirate scheme, the frequency spectra of the fairlead tensions were evaluated. Given that the excitation frequency of the imposed motion is 0.1Hz, and by comparison with the frequency spectra of the results from the stable singlerate scheme, the onset of instability corresponding to the set of multirate parameters can be determined. These input parameters are the partition timestep ratios α_c and α_f. The range for α_f is from 0.5 to 1.0, and the range of α_c is derived from the Partition C timestep F δt_c which must be a multiple, p, that of Partition F, δt_f. Thus δt_c and δt_f are the macro- and microsteps of the multirate integrator. Appendix B includes a sample of the total set of time signals for the R3 line in which the onset and development of instability is observed as a_c and a_f are increased. For the evaluation of accuracy, the results for maximum line tension and fairlead energy dissipation, as defined in Equation 23 where $T_{FL\,x}$ and f_x are the surge component of the fairlead tension and surge velocity respectively, are compared between the singlerate and multirate simulations. For the evaluation of computational efficiency, a comparison is made between the wall clock times for the singlerate simulation, which uses the maximum stable timestep of $\delta t_{f\max}$, and that of the multirate simulation.

$$\int_0^{t_X} T_{FL,x}\dot{r}_X \mathrm{dt} \tag{23}$$

Results and Discussion

Figure 5 and Figure 6 show the results of the stability analysis of the frequency spectra of the fairlead tension signal for discretizations E1 to E6, and R1 to R4 respectively, and where the stable and unstable fairlead tension results lie in terms of α_c and α_f. At lower values of α_c and α_f, the results are stable; even though the tests were conducted for $\alpha_c, \alpha_f \geq 0.5$, the stable region can be extrapolated to α_c, — 0 on the reasoning that instability is primarily a result of unstable timestep sizes in the base integration method or the applied multirate scheme.

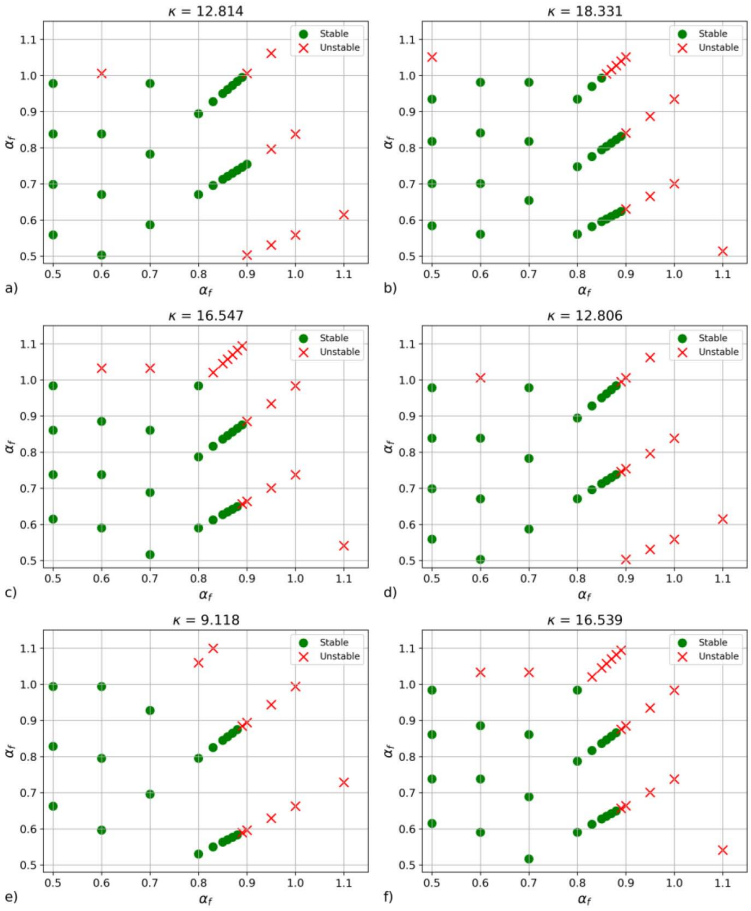

Figure 5—Stability plots for E1 (top-left), E2 (top-right), E3 (middle-left), E4 (middle-right), E5 (bottom-left), and E6 (bottom-right)

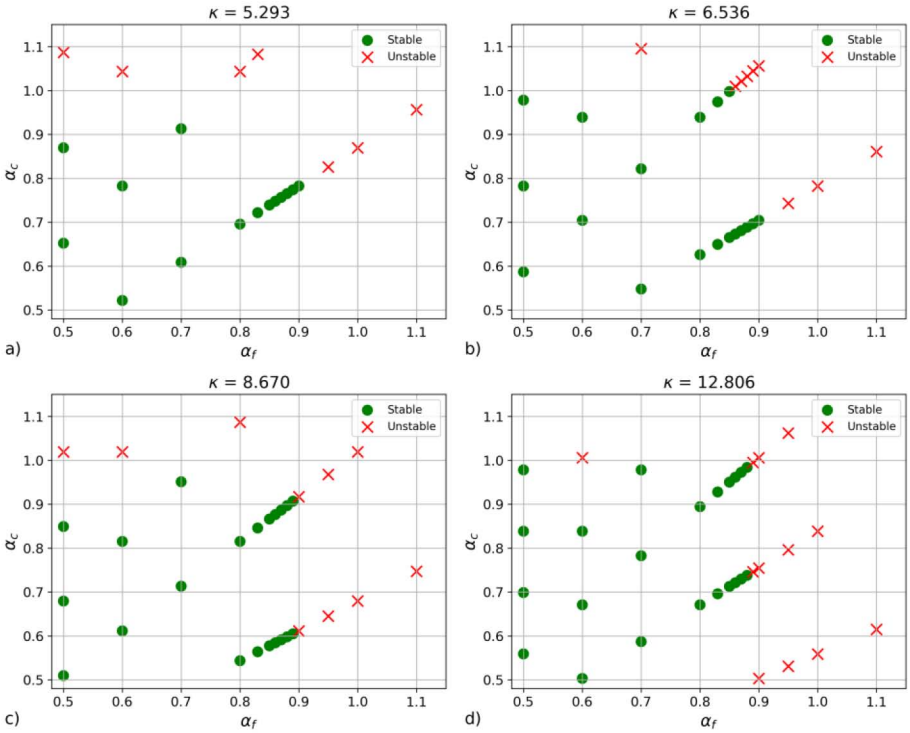

Figure 6—Stability plots for a) R1, b) R2, c) R3 and d) R4 lines

Overlaying the stability plots for the E1 to E6, as well as the R1 to R4, the stability regions arising from the variation of Partition F's length and nodal density is shown in Figure 7. An important factor for a multirate scheme is the stiffness ratio, κ, between coupled partitions, due to its influence on the number of microsteps required to achieve stability. Given that the series of tests were conducted for a range of stiffness ratios, $5.293 < \kappa < 12.806$, the stability map shown in Figure 7 indicates that the stable region is insensitive to the stiffness ratio, and that the stable region spans $\alpha_c < 1$, and $\alpha_f < 0.87$. There are several cases where stability is observed for $\alpha_f > 0.87$, however there are cases of instability as well, hence the upper stability limit of 0.87 is recommended for α_f.

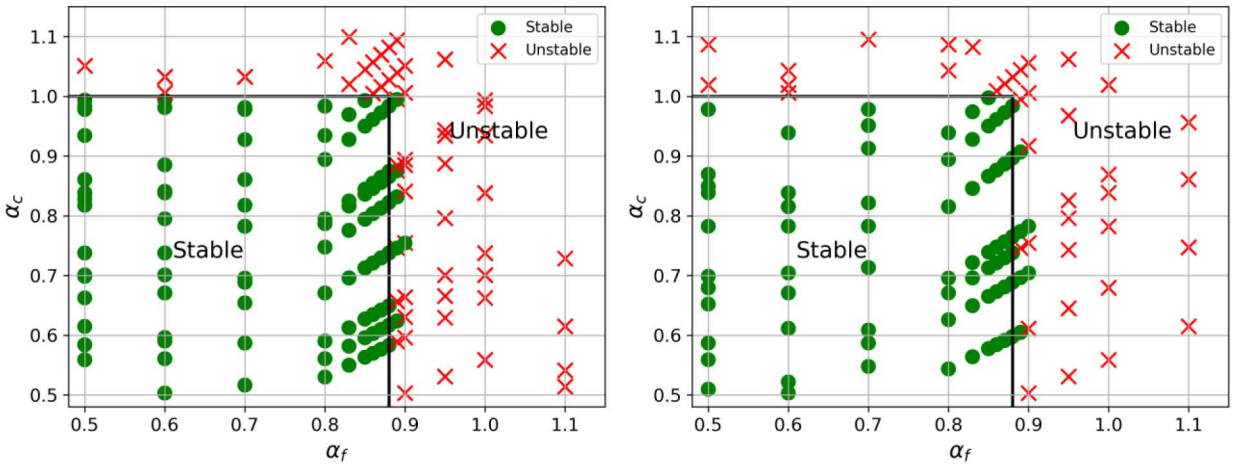

Figure 7—Stability regions from numerical experiments E1 to E6 (left) and R1 to R4 (right)

From this recommended stability range, and noting that the timestep ratio, p, between the micro- and macro-timesteps must be an integer value, the timesteps for the individual partitions can be chosen as,

$$\Delta t_f = \alpha_f \Delta t_{f,max}, \quad \alpha_f \leq 0.87$$
$$\Delta t_c = p\Delta t_f = \alpha_c \Delta t_{c,max}, \quad \alpha_c \leq 1, \; p \in \mathbb{Z}^+ \tag{24}$$

The accuracy of the multirate scheme is assessed by comparison to the results of the stable singlerate scheme and shown in Figure 8. The measures of accuracy were percentage deviation of the maximum tension and energy dissipation over one period of motion. The deviation of the maximum tension and energy dissipation of the multirate scheme from the singlerate was within 5.5% and 2% magnitude. This indicates that the multirate scheme, with the potential of reducing computational costs, produces results that are comparable in accuracy to the singlerate base integration method which uses a small timestep for the entire structure.

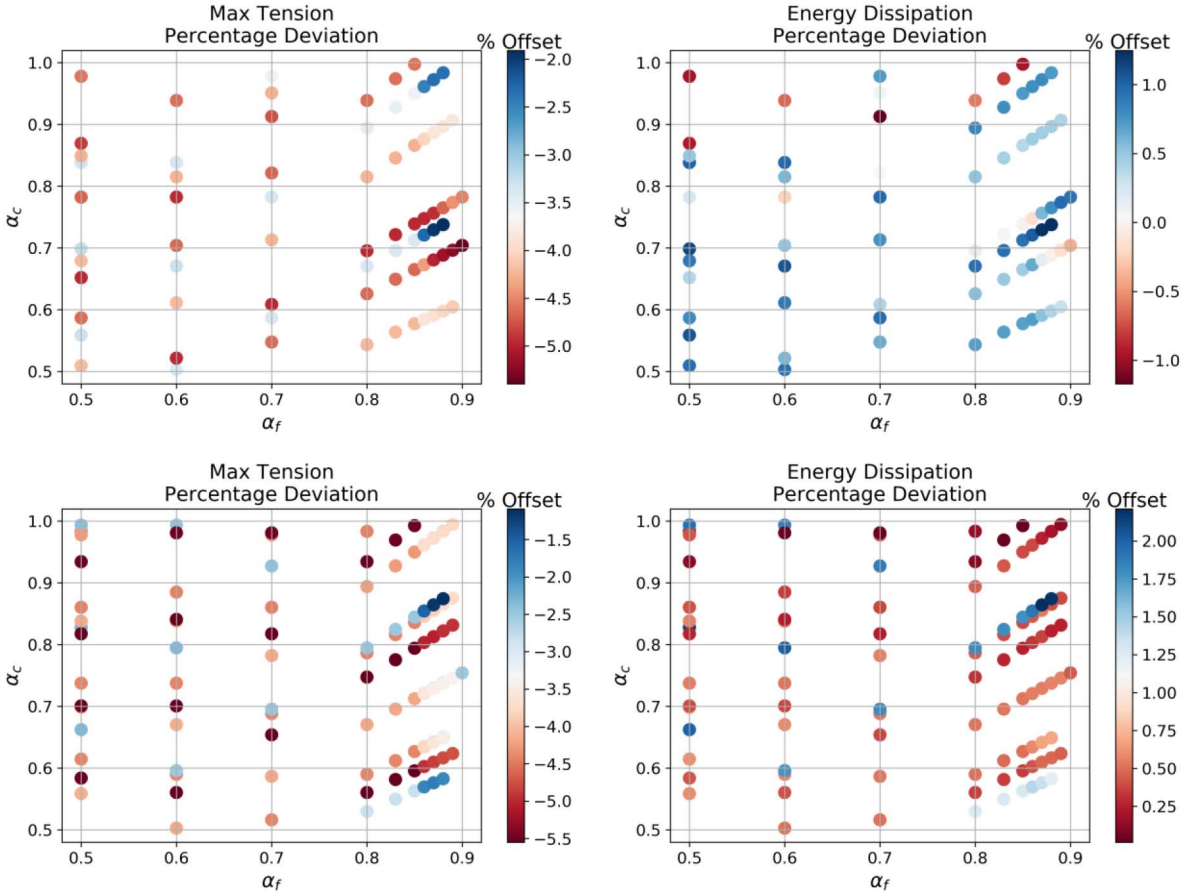

Figure 8—Percentage deviation of maximum tension and energy dissipation of multirate from singlerate results for R1 to R4 (top row) and E1 to E6 (bottom row)

The efficiency of the multirate scheme is given by computational speedup parameter, β as defined in Table 1. The results for E1 to E6, corresponding to an enlargement of Partition F, are dotted in Figure 9. The results for R1 to R4, corresponding to a progressive refinement in Partition F nodal density, and increase in stiffness factor, κ, are shown in Figure 10. The plots show that computational speedup is achievable for all the cases with a maximum speedup of 1.93, which corresponds to almost a halving of the computational time taken by the singlerate method. However, it is observed with the enlargement of Partition F, which is advanced using smaller timesteps, the speedup is reduced. Another observation is that larger speedups are achieved with larger α_f and α_c within the stability bounds. Given that the errors in the accuracy of the

multirate method is low across the range of α_f and α_c, as shown in Figure 8, it is thus advisable to use the largest possible α_f and α_c values.

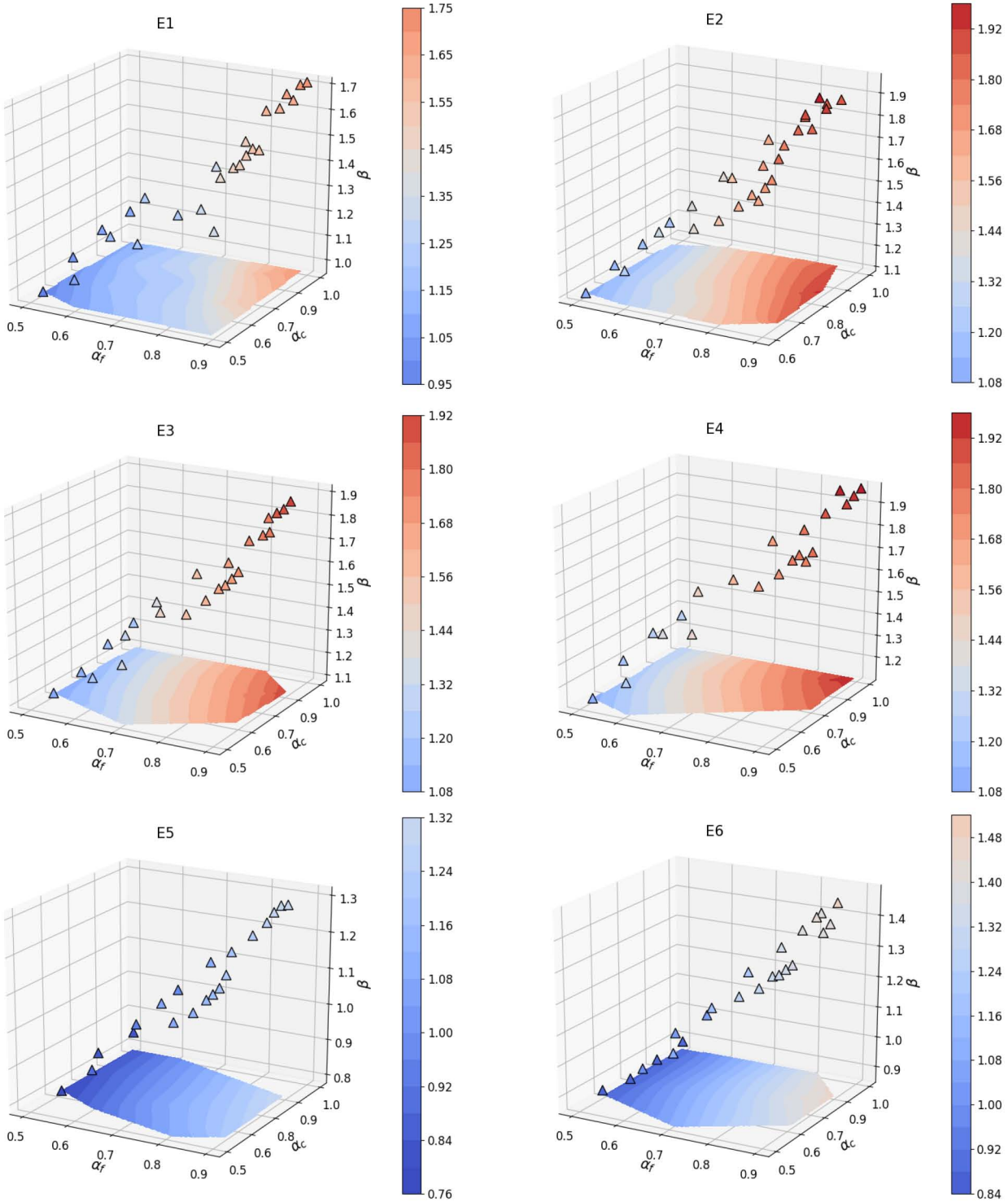

Figure 9—Speedup, β, for E1 to E6 cases

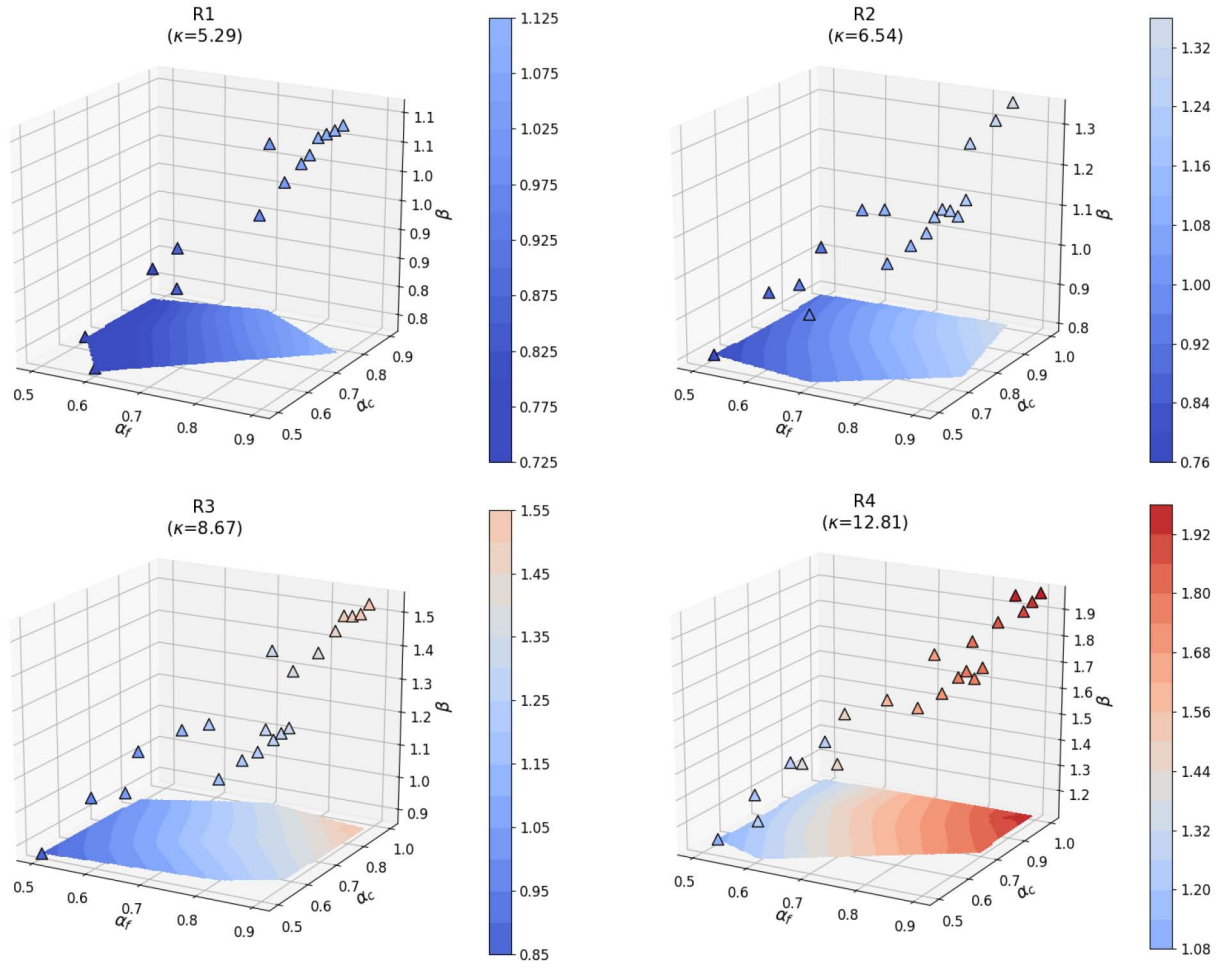

Figure 10—Speedup, β, for R1 to R4 cases

Having established that the stability region for this multirate scheme is as shown in Equation 24, and that the accuracy of the multirate method is low across the stable a_f and a_c range, the recommended values for a_f and a_c in the present multirate method for a two-partition system can be summarized as,

$$\alpha_f = 0.87$$
$$\alpha_c = 1.0 \tag{25}$$

For a multiple partition system, an inference may be made that the recommended values will hold, with a_f and a_c conditions applied to any two interfacing partitions.

Conclusion

A multirate time integration method based on a staggered, sequential approach, and paired with the Modified Euler integration method was proposed. The benefits of using this combination of methods is that the Modified Euler procedure does not rely on intermediate stage function evaluations This allows the slower partition to be advanced in time without relying extrapolation methods to obtain the coupled state variable values in the coupled partition. When subsequently advancing the fast partition, interpolation in time can be used to obtain the state values from the slow partition. A stability analysis of the method was performed using numerical experiments leading to a set of stability parameters and a method to determine suitable stable timesteps for the coupled partitions. An accuracy analysis was performed comparing the multirate and singlerate method which uses the smaller stable timestep and it was found that the results, when the

stability constraints were applied, compared very well to the singlerate method. Finally, it was found that the method can produce good computational speedup when the stability parameters were applied, thus allowing a set of recommended values to be proposed for the each of the stability parameters that will yield good accuracy and maximum speedup.

Acknowledgements

This study received financial support from the EDB-IPP programme and Lloyd's Register. The authors would especially like to thank Dr. Frank Lin and Mr. Kim Youngkook, from Lloyd's Register Applied Technology Group and Global Technology Center Singapore respectively, for their valuable input.

References

Andrus, J. F. (1979). Numerical Solution of Systems of Ordinary Differential Equations Separated into Subsystems. *SIAM Journal on Numerical Analysis*, **16**(4), 605–611.

Arnold, M. (2007). Multi-Rate Time Integration for Large Scale Multibody System Models. In P. Eberhard (Ed.), IUTAMSymposium on Multiscale Problems in Multibody System Contacts: Proceedings of the IUTAM Symposium held in Stuttgart, Germany, February 20-23, 2006 (pp. 110). http://doi.org/10.1007/978-1-4020-5981-0_1

Bai, Y. (2001). *Pipelines and Risers*. (R. Bhattacharyya & M. E. McCormick, Eds.). Oxfordshire, UK: Elsevier.

Bartel, A. (2001). Multirate ROW methods of mixed type for circuit simulation. *Scientific Computing in Electrical Engineering*, **18**(1), 241–249.

Bartel, A., Gunther, M., & Rentrop, P. (2002). Numerical Techniques for Different Time Scales in Electric Circuit Simulation. In M. Breuer, F. Durst, & C. Zenger (Eds.), *High Performance Scientific And Engineering Computing. Lecture Notes in Computational Science and Engineering* (pp. 343–360). Springer, Berlin, Heidelberg.

Bathe, K. J. (1996). *Finite Element Procedures* (2nd ed.). New Jersey, USA: Prentice-Hall, Inc.

Boom, H. J. J. Van Den. (1985). Dynamic Behaviour of Mooring Lines. In 4th International Conference on Behaviour of Offshore Structures (pp. 359–368). Delft, the Netherlands.

Brown, D. T., & Mavrakos, S. (1999). Comparative study on mooring line dynamic loading. *Marine Structures*, **12**, 131–151.

C. Webster, W. (1995). Mooring-induced damping. *Ocean Engineering*, **22**(6), 571–591. http://doi.org/10.1016/0029-8018(94)00027-5

Chang, J., Ploen, S., Sohl, G., & Martin, B. (2004). Parallel Multi-Step/Multi-Rate Integration of Two-Time Scale Dynamic Systems. In AIAA Modeling and Simulation Technologies Conference and Exhibit. Providence, Rhode Island, USA. http://doi.org/10.2514Z6.2004-5162

Chang, Z., Tang, Y., Li, H., Yang, J., & Wang, L. (2012). Analysis for the deployment of single-point mooring buoy system based on multi-body dynamics method. *China Ocean Engineering*, **26**(3), 495–506. http://doi.org/10.1007/s13344-012-0037-x

Det Norske Veritas. (2003). *Composite Risers (DNV-RP-F202)*. Høvik, Norway: Det Norske Veritas. Retrieved from http://www.dnv.com

Elosta, H., Shan Huang, & Atilla Incecik. (2016). Seabed Interaction Modeling Effects on the Global Response of Catenary Pipeline : A Case Study. *Journal of Offshore Mechanics and Arctic Engineering*, **136**(August 2014), 1–8. http://doi.org/10.1115/L4027177

Elsacker, A. W. Van. (1989). The Behaviour of Flexible Risers in Waves. In Proceedings of the Offshore Technology Conference, Houston, Texas (pp. 515–524).

Gander, M. J., & Halpern, L. (2013). Techniques for Locally Adaptive Time Stepping Developed over the Last Two Decades. In *Domain Decomposition Methods in Science and Engineering XX*.

Lecture Notes in Computational Science and Engineering (Vol. **91**). Springer, Berlin, Heidelberg.

Gear, C. W., & Wells, D. R. (1984). Multirate linear multistep methods. *BIT Numerical Mathematics*, **24**(4), 484–502. http://doi.org/10.1007/BF01934907

Ghadimi, R. (1988). A simple and efficient algorithm for the static and dynamic analysis of flexible marine risers. *Computers & Structures*, **29**, 541–555.

Gobat, J. I. (2000). *The Dynamics of Geometrically Compliant Mooring Systems* (PhD thesis). Massechusetts Institute of Technology and Woods Hole Oceanographic Institution.

Gunther, M., Kværno, A., & Rentrop, P. (2001). Multirate Partitioned Runge-Kutta Methods. *BIT Numerical Mathematics*, **41**(3), 504–514. http://doi.org/10.1023/A:1021967112503

Gunther, M., & Rentrop, P. (1993). Multirate ROW methods and latency of electric circuits. *Applied Numerical Mathematics*, **13**(1-3), 83–102. http://doi.org/10.1016/0168-9274(93)90133-C

Hahn, G. D. (1991). A modified Euler method for dynamic analyses. *International Journal for Numerical Methods in Engineering*, **32**(March 1990), 943–955. Retrieved from http://onlinelibrary.wiley.com/doi/10.1002/nme.1620320502/abstract

Huang, S., & Vassalos, D. (1993). A numerical method for predicting snap loading of marine cables. *Applied Ocean Research*, **15**, 235–242.

Hull, T. E., Enright, W. H., & Fellen, B. M. (1972). Comparing Numerical Methods for Ordinary Differential Equations. *SIAM Journal on Numerical Analysis*, **9**(4), 603–636.

Kavaerno, A., & Rentrop, P. (1999). *Low order multirate Runge-Kutta methods in electric circuit simulation* (Preprint. Institute for Scientific Computing and Mathematical Modeling, University of Karlsruhe; 1,999.1). Karlsruhe.

Kurian, V. J., Yassir, M. A., Ng, C. Y., & Harahap, I. S. (2013). Nonlinear dynamic analysis of multicomponent mooring lines incorporating line-seabed interaction. *Research Journal of Applied Sciences, Engineering and Technology*, **6**(8), 1428–1445.

Leyendecker, S., & Ober-Blobaum, S. (2013). *A Variational Approach to Multirate Integration for Constrained Systems*, 97–121. http://doi.org/10.1007/978-94-007-5404-1

Liu, Y., & Bergdahl, L. (1997). Influence of current and seabed friction on mooring cable response: Comparison between time-domain and frequency-domain analysis. *Engineering Structures*, **19**(11), 945–953. http://doi.org/10.1016/S0141-0296(97)00176-4

Low, Y. M., & Langley, R. S. (2008). A hybrid time/frequency domain approach for efficient coupled analysis of vessel/mooring/riser dynamics. *Ocean Engineering*, **35**, 433–446. http://doi.org/10.1016Zj.oceaneng.2008.01.001

Shome, S. S., Haug, E. J., & Jay, L. O. (2004). Dual-Rate Integration Using Partitioned Runge-Kutta Methods for Mechanical Systems with Interacting Subsystems. *Mechanics Based Design of Structures andMachines*, **32**(3), 253–282. http://doi.org/10.1081/LMBD-200027930

Thomas, D. (1993). *A Numerical Investigation of Time Schemes Applied to the Dynamic Solution of Mooring Lines* (PhD thesis). The University of Newcastle upon Tyne.

Tomulik, P., & Fræczek, J. (2011). Simulation of multibody systems with the use of coupling techniques: A case study. *Multibody System Dynamics*, **25**(2), 145–165. http://doi.org/10.1007/s11044-010-9206-y

Verhoeven, A., Guennouni, A. E., ter Maten, E. J. W., & Mattheij, R. M. M. (2005). Multirate methods for the transient analysis of electrical circuits. *PAMM (Proc ApplMath Mech)*, **5**, 821–822.

Webster, W. C. (1995). Mooring-induced damping. *Ocean Engineering*, **22**(6), 571–591. http://doi.org/10.1016/0029-8018(94)00027-5

Yu, L., & Tan, J. H. (2006). Numerical investigation of seabed interaction in time domain analysis of mooring cables. *Journal of Hydrodynamics*, **18**(4), 424–430. http://doi.org/10.1016/S1001-6058(06)60115-7

Appendix A

Test Case Mooring Line Discretization

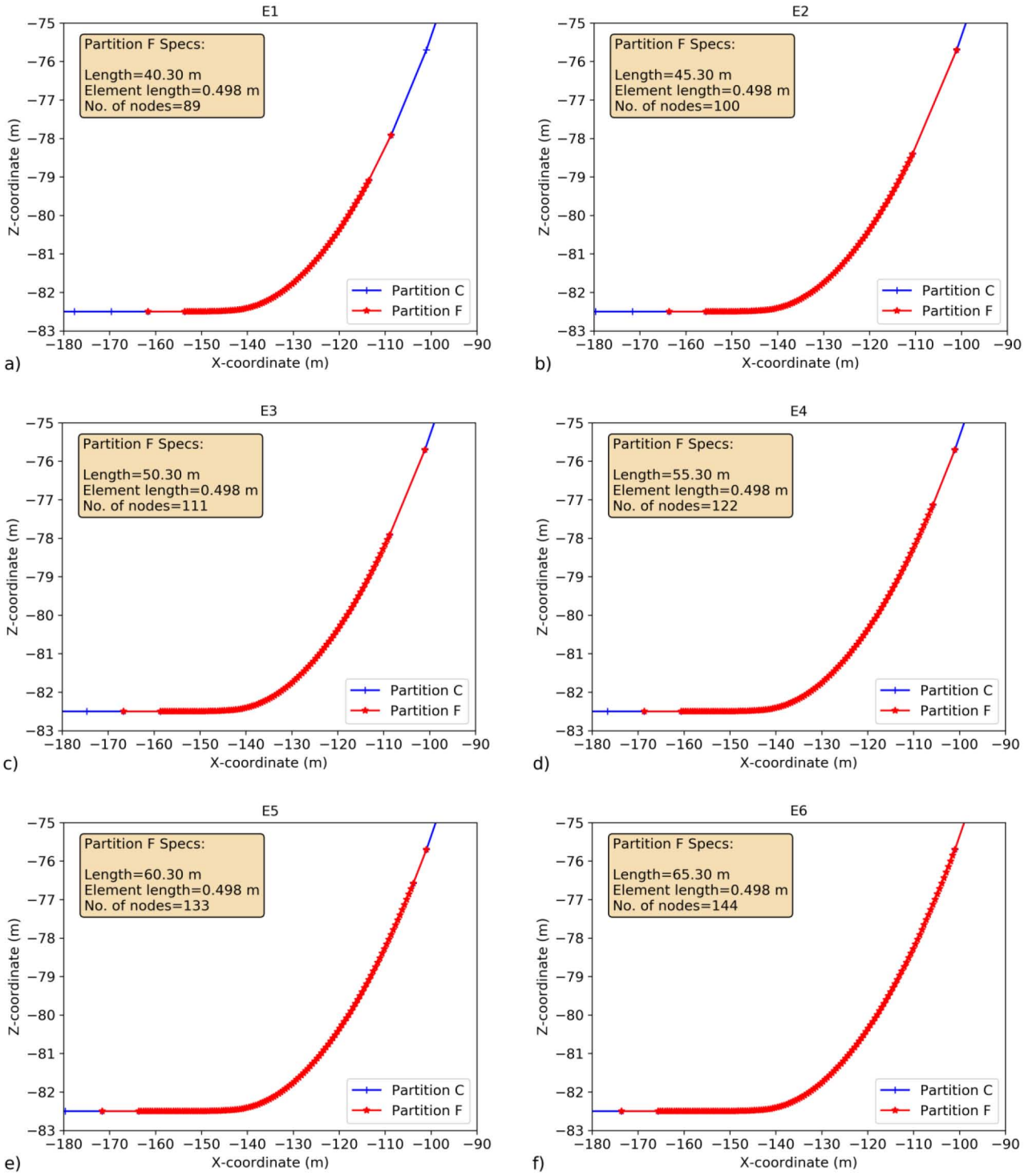

Figure A 1—Close-up of Partition F with a length of a) 40.3m, b) 45.3m, c) 50.3, d) 55.3m, e) 60.3m and f) 65.3m

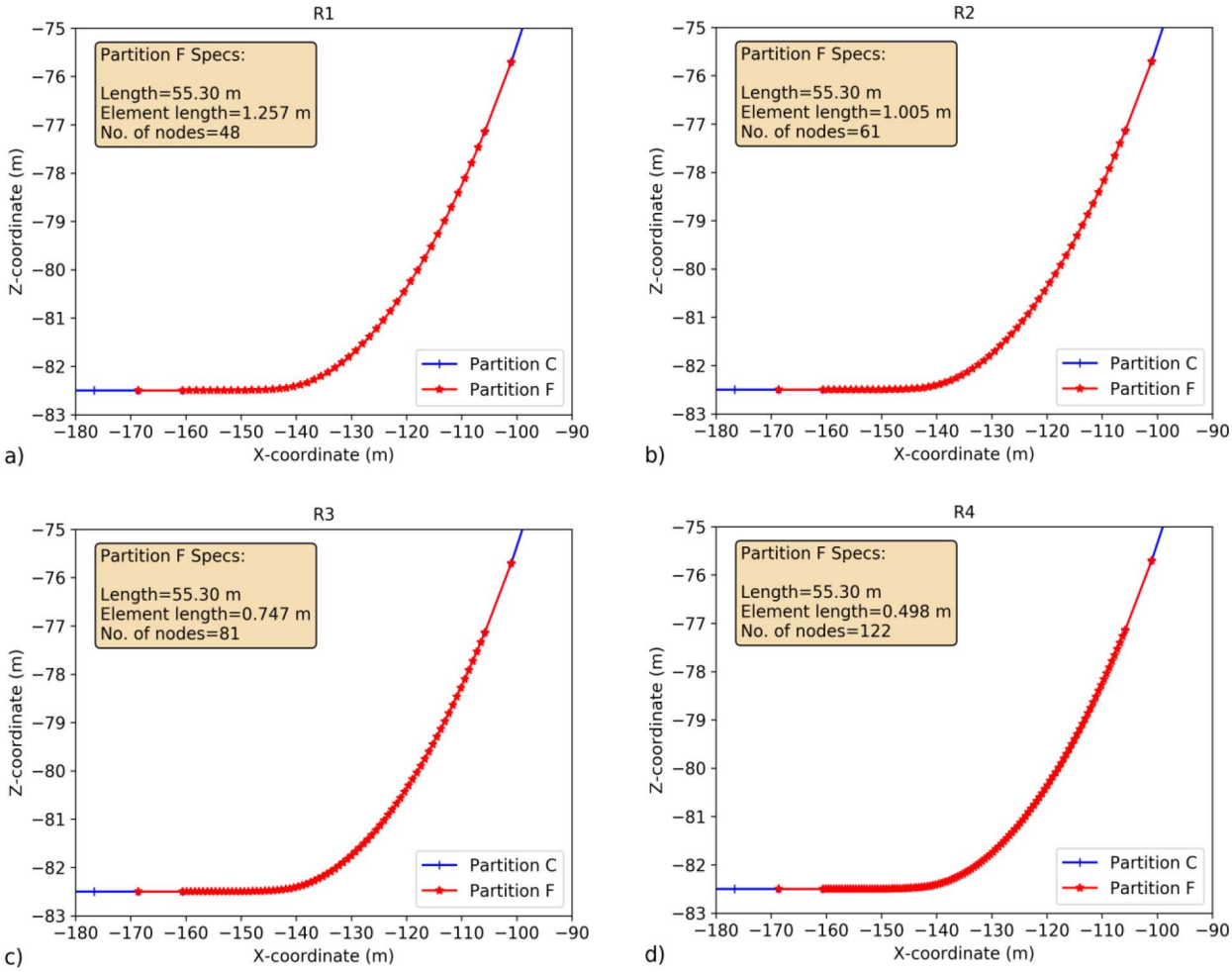

Figure A 2—Close-up of Partition F with a length of 55.3 m and a) R1, b) R2, c) R3 and d) R4 discretizations

Appendix B

Examples of Fairlead Tension Time Signals for Stable and Unstable Cases

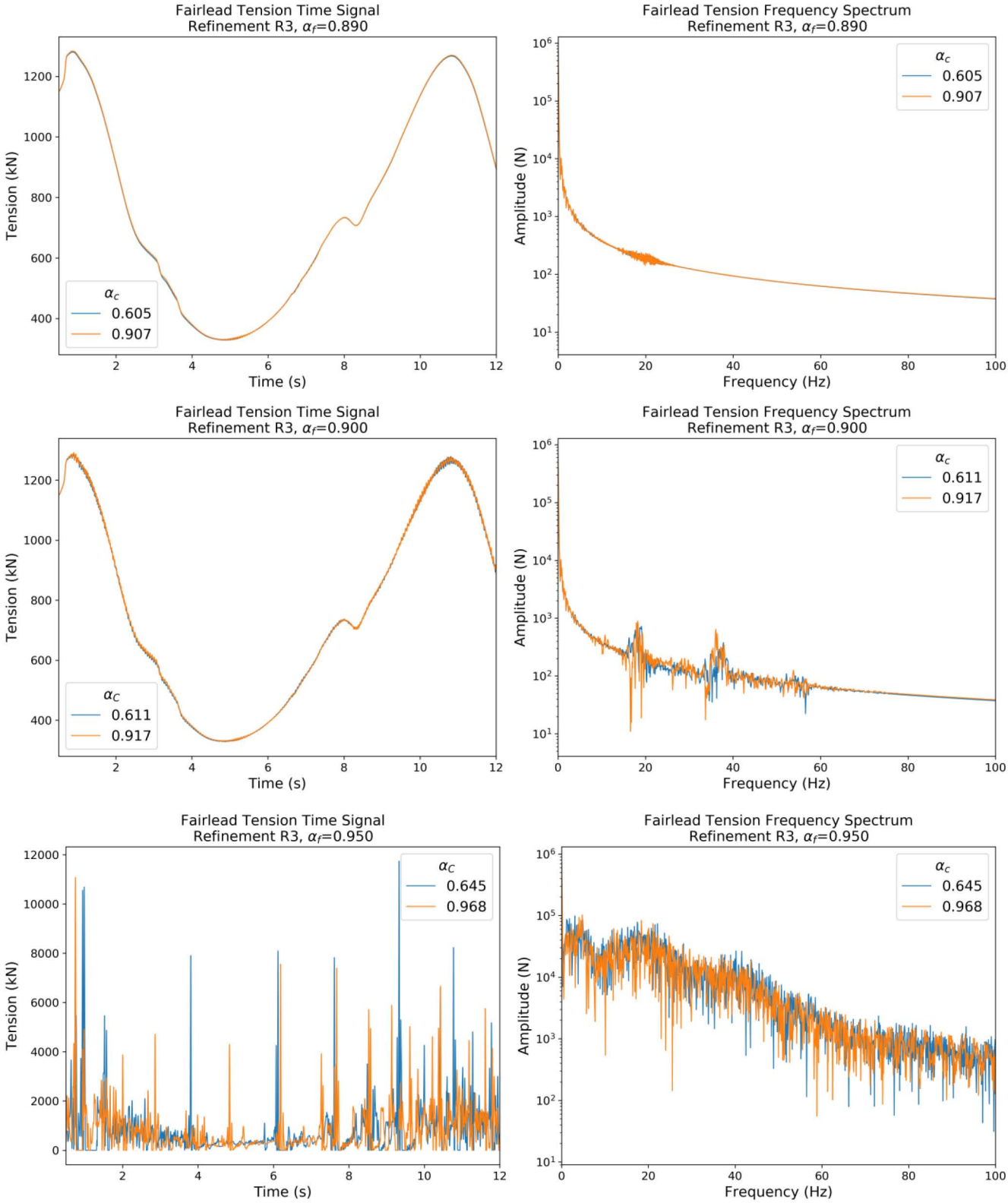

Figure B 1—Fairlead tension time signal and frequency spectrum with stable (top), slightly unstable (middle) and unstable